Temporal-callosal pathway diffusivity predicts phonological skills in children

Robert F. Dougherty, Michal Ben-Shachar, Gayle K. Deutsch, Arvel Hernandez, Glenn R. Fox, and Brian A. Wandell

PNAS 2007;104;8556-8561; originally published online May 4, 2007;
doi:10.1073/pnas.0608961104

Temporal-callosal pathway diffusivity predicts phonological skills in children

Robert F. Dougherty*, Michal Ben-Shachar, Gayle K. Deutsch, Arvel Hernandez, Glenn R. Fox, and Brian A. Wandell

Stanford Institute for Reading and Learning, and Department of Psychology, Stanford University, Stanford, CA 94305

Edited by Marcus E. Raichle, Washington University School of Medicine, St. Louis, MO, and approved April 3, 2007 (received for review October 10, 2006)

The development of skilled reading requires efficient communication between distributed brain regions. By using diffusion tensor imaging, we assessed the interhemispheric connections in a group of children with a wide range of reading abilities. We segmented the callosal fibers into regions based on their likely cortical projection zones, and we measured diffusion properties in these segmented regions. Phonological awareness (a key factor in reading acquisition) was positively correlated with diffusivity perpendicular to the main axis of the callosal fibers that connect the temporal lobes. These results could be explained by several physiological properties. For example, good readers may have fewer but larger axons connecting left and right temporal lobes, or their axon membranes in these regions may be more permeable than the membranes of poor readers. These measurements are consistent with previous work suggesting that good readers have reduced interhemispheric connectivity and are better at processing rapidly changing visual and auditory stimuli.

corpus callosum | diffusion tensor imaging | magnetic resonance imaging | reading

Reading is a crucial skill in modern industrialized societies. Therefore, it is important to understand how people learn, or fail to learn, this skill. A substantial behavioral and neuroscience literature characterizes the neural basis of reading in both children and adults. Functional neuroimaging studies of reading have identified a distributed functional network where neural activity correlates with reading skill (1–5).

Such a distributed network of cortical regions requires a set of long-range white matter tracts to communicate essential signals. Structural neuroimaging studies using diffusion tensor imaging (DTI) have identified white matter properties that vary with reading skill. Klingberg *et al.* (6) were the first to apply DTI in the study of reading disabilities. They compared fractional anisotropy (FA) (a measure of the diffusion anisotropy within the white matter) in reading-impaired and normal-reading adults. They found a statistically significant difference primarily in a left temporal-parietal region of the white matter. This basic result has been replicated and extended to children by three independent groups (7–9).

In addition to these recent measurements of the white matter using DTI, there is also a long history of measurements and theories arguing for a relationship between interhemispheric communication and reading (10–15). Orton (10) proposed that the lack of left-hemisphere language dominance was the cause of dyslexia. Geschwind and colleagues (11, 16) also argued that reduced left-hemisphere dominance was a cause of dyslexia. More recent measurements using structural MRI suggest that the corpus callosum has a different shape in dyslexic adults compared with those with normal reading development (17–19). Other research on the callosum supports the basic idea that increased functional (20) and structural (21) hemispheric asymmetry is associated with sparser interhemispheric connectivity, thus providing a logical connection between callosal morphology and hemispheric symmetry.

Given the sensitivity of DTI to white matter differences, it is surprising that previous DTI studies of reading did not find differences in the corpus callosum. However, as we have shown, there is high variance and thus low statistical power for tests of diffusion anisotropy in the corpus callosum when standard voxel-based methods are used (22). To overcome this problem, in this study we used a region of interest (ROI)-based approach to measure diffusion properties in the corpus callosum.

Here, we describe DTI measurements that establish a correlation between diffusion properties in the posterior corpus callosum and phonological awareness, a key factor in reading acquisition. In a large group of children, we manually segmented the corpus callosum in each brain according to estimated cortical projection zones. We found that high phonological awareness is associated with higher diffusivity in the directions perpendicular to the main fiber direction (radial diffusivity) primarily in pathways that connect the temporal lobes. We consider several biological mechanisms that might cause this difference in radial diffusivity.

Results

Callosal shapes and sizes vary significantly across subjects so that segmentation based on shape may not follow function. Furthermore, the positions of pathways projecting to functionally distinct regions do not correlate well with the gross callosal morphology (22). For example, the splenium, traditionally defined as the region posterior to the narrowing (isthmus) of the callosum (23), includes fibers with projection zones in temporal, parietal, and occipital lobes. For these reasons, we manually segmented the callosum based on estimated cortical projection zone (see *Methods*) and analyzed diffusion properties in the identified callosal segments.

We computed the FA and mean diffusivity (MD) values within the fiber pathways passing through each callosal segment in each subject. A 2-cm length of each callosal fiber, 1 cm to the left and right of the midsagittal plane, was identified, and the tensors closest to each point along the pathways were extracted. The FA and MD values were computed from these tensors. A tensor may be included in more than one callosal segment; the FA and MD estimates for each fiber group form weighted averages. For example, voxels intersected by many fibers from a particular callosal segment contribute more to the mean of that segment than voxels intersected by just a few fibers from that segment.

We compared several behavioral measures with the mean FA (Table 1) and MD (Table 2) of each of the seven callosal segments. The strongest correlation was between phonological awareness and FA in the temporal-callosal segment ($r = -0.51$; $P < 0.0002$). There were also substantial correlations with word attack and passage comprehension, although only the correlation between phonological awareness and FA in the temporal segment was significant with a family-wise $P < 0.05$ after applying a Bonferroni correction for

Author contributions: R.F.D., M.B.-S., G.K.D., and B.A.W. designed research; R.F.D., M.B.-S., G.K.D., and A.H. performed research; R.F.D. contributed new reagents/analytic tools; R.F.D., A.H., and G.R.F. analyzed data; and R.F.D., M.B.-S., and B.A.W. wrote the paper.

The authors declare no conflict of interest.

This article is a PNAS Direct Submission.

Abbreviations: DTI, diffusion tensor imaging; FA, fractional anisotropy; ROI, region of interest; MD, mean diffusivity; ADHD, attention deficit/hyperactivity disorder; PDD, principal diffusion direction; AC, anterior commissure; PC, posterior commissure.

*To whom correspondence should be addressed. E-mail: bobd@stanford.edu.

Table 1. Callosal segment FA correlations (Pearson's *r*) with behavioral measures

	Occ	Temp	PostPar	SupPar	SupFront	AntFront	Orb
Letter-word ID	−0.08	−0.19	−0.22	−0.2	−0.12	−0.08	−0.15
	(−0.38, 0.45)	(−0.47, 0.38)	(−0.45, 0.32)	(−0.48, 0.43)	(−0.37, 0.14)	(−0.34, 0.3)	(−0.42, 0.53)
Word attack	−0.18	−0.34	−0.16	−0.13	−0.11	0.03	−0.2
	(−0.44, 0.35)	(−0.59, 0.37)	(−0.42, 0.5)	(−0.43, 0.49)	(−0.35, 0.16)	(−0.25, 0.27)	(−0.45, 0.37)
Passage comprehension	−0.25	−0.43*	−0.27	−0.14	−0.05	−0.13	−0.22
	(−0.53, 0.4)	(−0.64, −0.27)	(−0.51, 0.47)	(−0.39, 0.41)	(−0.29, 0.12)	(−0.46, 0.53)	(−0.47, 0.35)
Phonological awareness	−0.31	−0.51**	−0.22	−0.29	−0.16	−0.06	−0.22
	(−0.57, 0.38)	(−0.71, −0.41)	(−0.44, −0.12)	(−0.54, 0.28)	(−0.4, 0.01)	(−0.32, 0.48)	(−0.46, 0.4)
Rapid naming	0.17	0.08	0.08	0.17	0.11	−0.04	0.01
	(−0.05, 0.3)	(−0.2, 0.68)	(−0.2, 0.58)	(−0.12, 0.67)	(−0.17, 0.31)	(−0.34, 0.46)	(−0.29, 0.47)
Phonological memory	0.06	0.05	−0.29	−0.18	−0.17	−0.32	−0.17
	(−0.26, 0.69)	(−0.19, 0.54)	(−0.56, 0.45)	(−0.42, 0.37)	(−0.44, 0.04)	(−0.58, 0.27)	(−0.39, 0.12)
GORT-4 Reading Quotient	−0.15	−0.27	−0.27	−0.11	−0.2	−0.06	−0.25
	(−0.44, 0.42)	(−0.49, 0.35)	(−0.54, 0.44)	(−0.39, 0.49)	(−0.44, 0.4)	(−0.33, 0.64)	(−0.49, 0.36)
WISC–IV Full-Scale IQ	−0.13	−0.18	−0.18	0.08	0.05	−0.08	0.06
	(−0.41, 0.43)	(−0.45, 0.4)	(−0.43, 0.36)	(−0.2, 0.64)	(−0.18, 0.15)	(−0.36, 0.52)	(−0.21, 0.76)

*, $P < 0.01$; **, $P < 0.001$. The 95% confidence intervals (estimated from 1,000 bootstrap samples) are indicated in parentheses. Occ, occipital; Temp, temporal; PostPar, posterior parietal; SupPar, superior parietal; SupFront, superior frontal; AntFront, anterior frontal; Orb, orbitofrontal.

112 planned statistical comparisons; this conservative correction results in a family-wise critical *r* of 0.48. Phonological awareness was strongly correlated with word attack ($r = 0.68$) and passage comprehension ($r = 0.70$), and partial correlation analysis indicated that all three measures accounted for the same variance in the temporal-callosal FA. We focus subsequent analyses on phonological awareness, but acknowledge that the discussion could similarly apply to these other measures of reading. We should also note that there were no statistically reliable sex differences and no reliable correlations with the Conners' ADHD Index. There was a modest positive correlation between age and FA in the temporal-callosal segment ($r = 0.30$; $P = 0.04$), but a partial correlation analysis showed that controlling for age had a negligible effect on the phonological awareness correlation in this region ($r = -0.48$ after controlling for age).

The individual measurements producing the FA correlations in the temporal segment and three nearby segments (occipital, posterior parietal, and superior parietal) are plotted in Fig. 1.

We also analyzed the correlations between MD and behavior in these same callosal segments. The highest correlations between MD and behavioral measures (Table 2) were found in the same temporal-callosal segment. There was also a modest correlation in the orbitofrontal segment with passage comprehension.

The pattern of lower FA and higher MD in the temporal-callosal segment in good readers could be caused by several possible differences in the tensor shapes. To clarify the observed differences, we made further analyses of the tensors in the temporal-callosal segment.

The diffusion tensor can be represented as an ellipsoid where a proton at the center of the voxel has an equal probability of diffusing to any point on that ellipsoid. The eigenvectors of the diffusion tensor represent the three axes of the ellipsoid (see Fig. 2*A*). The three eigenvalues (λ_i) represent the apparent diffusion coefficient (or simply "diffusivity") along each of these three directions. The eigenvector corresponding to the largest eigenvalue (λ_1), which represents the longest axis of the ellipsoid, is called the principal diffusion direction (PDD). The ellipsoid axis length along the PDD is the $\sqrt{\lambda_1}$.

In the case of the corpus callosum, we expect the PDD to be oriented consistently along the left–right axis. The data bear this prediction out: The mean PDD in the midsagittal plane of the callosum was within 3° of the left–right axis in all of the posterior

Table 2. Callosal segment MD correlations with behavioral measures

	Occ	Temp	PostPar	SupPar	SupFront	AntFront	Orb
Letter-word ID	0.1	0.3	0.24	0.32	0.21	0.26	0.28
	(−0.19, 0.67)	(−0.01, 0.78)	(−0.06, 0.74)	(0.04, 0.73)	(−0.041, 0.37)	(−0.04, 0.69)	(0.021, 0.39)
Word attack	0.07	0.39*	0.22	0.3	0.28	0.22	0.28
	(−0.23, 0.64)	(0.1, 0.84)	(−0.06, 0.42)	(0.03, 0.78)	(0.04, 0.4)	(−0.06, 0.73)	(0.0, 0.56)
Passage comprehension	0.11	0.42*	0.13	0.25	0.14	0.29	0.43*
	(−0.22, 0.72)	(0.17, 0.58)	(−0.17, 0.81)	(−0.024, 0.47)	(−0.11, 0.37)	(−0.07, 0.94)	(0.16, 0.59)
Phonological awareness	0.11	0.46**	0.22	0.33	0.27	0.11	0.35
	(−0.25, 0.71)	(0.18, 0.61)	(−0.12, 0.8)	(0.01, 0.82)	(0.04, 0.38)	(−0.25, 0.79)	(0.01, 0.85)
Rapid naming	−0.12	−0.01	−0.16	−0.03	−0.06	0.04	−0.13
	(−0.32, −0.048)	(−0.23, 0.13)	(−0.4, −0.04)	(−0.24, 0.1)	(−0.3, 0.24)	(−0.2, 0.23)	(−0.37, 0.41)
Phonological memory	0.08	0.14	0.21	0.25	0.091	0.25	0.07
	(−0.23, 0.62)	(−0.1, 0.26)	(−0.06, 0.4)	(−0.02, 0.77)	(−0.15, 0.66)	(−0.05, 0.73)	(−0.21, 0.63)
GORT-4 Reading Quotient	0.01	0.23	0.14	0.24	0.24	0.25	0.28
	(−0.27, 0.21)	(−0.06, 0.62)	(−0.14, 0.64)	(−0.04, 0.69)	(−0.01, 0.4)	(0.01, 0.43)	(0.0, 0.54)
WISC–IV Full-Scale IQ	−0.01	0.17	−0.01	−0.06	−0.04	0.03	0.2
	(−0.22, 0.06)	(−0.06, 0.27)	(−0.29, 0.54)	(−0.28, 0.03)	(−0.26, 0.04)	(−0.29, 0.61)	(−0.1, 0.71)

Conventions are the same as in Table 1. Occ, occipital; Temp, temporal; PostPar, posterior parietal; SupPar, superior parietal; SupFront, superior frontal; AntFront, anterior frontal; Orb, orbitofrontal.

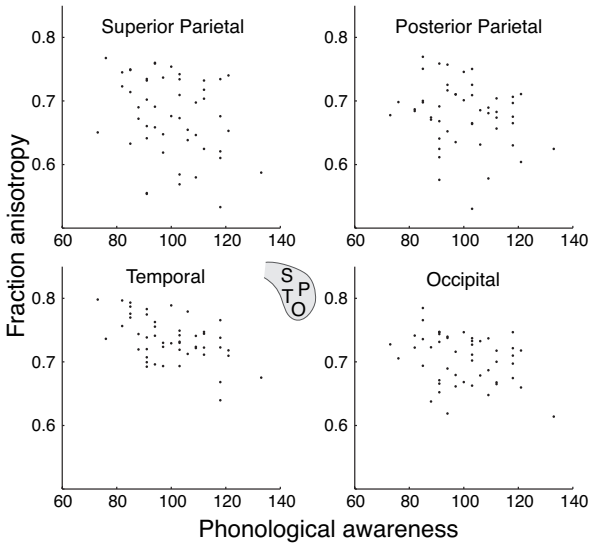

Fig. 1. FA and phonological awareness scatterplots for the four posterior callosal regions. The *Inset* icon shows the rough location of each of the four regions: superior parietal (S), posterior parietal (P), temporal (T), and occipital (O).

callosal segments of all subjects. The angular dispersion, a measure of the direction variance (24), was <5° within and across subjects, further indicating the high directional coherence in this callosal region.

We next analyzed the relationship between the individual eigenvalues λ_i and phonological awareness (Fig. 2*B*). The first eigenvalue (λ_1), which represents diffusivity along the left–right axis of the brain, was substantially higher than the second (λ_2) and third (λ_3) eigenvalues and was not correlated with phonological awareness ($r = 0.15$; $P > 0.2$). The second and third eigenvalues were significantly correlated with phonological awareness ($r = 0.46$ and $P = 0.001$ for λ_2; $r = 0.57$ and $P < 0.0001$ for λ_3).

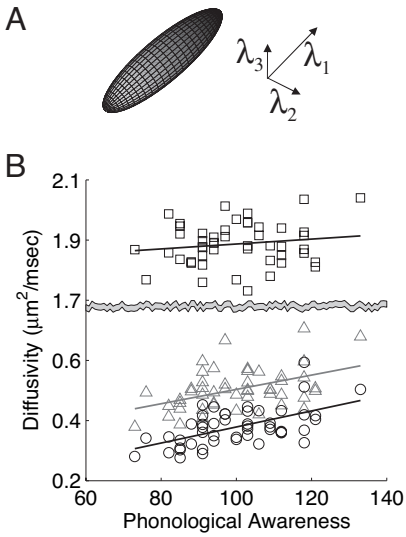

Fig. 2. Eigenvalue analysis of the temporal-callosal segment. (*A*) The ellipsoid representation of the diffusion tensor. The first eigenvalue represents the diffusivity along the longest axis of the ellipsoid, the second represents the diffusivity along the next longest axis, and the third represents diffusivity along the shortest axis of the ellipsoid. (*B*) The FA and MD correlations with phonological awareness are carried by the second (triangles) and third (circles) eigenvalues. The first eigenvalue (squares) is not correlated with phonological awareness. For reference, note that the typical MD in the nearby cerebrospinal fluid was roughly equivalent to that of freely diffusing water at body temperature [3 μm^2/msec (50)].

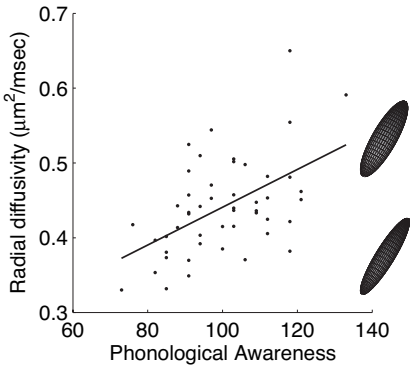

Fig. 3. Radial diffusivity and phonological awareness in the temporal-callosal segment accounted for 27% of the behavioral variance ($r = 0.52$; $P < 0.0002$; df = 47). Radial diffusivity was computed as the mean of the second and third eigenvalues.

The second and third eigenvalues were of similar magnitude, highly correlated ($r = 0.91$), and the corresponding eigenvalues randomly oriented both within and across subjects, suggesting that the diffusion ellipsoid in this region is radially symmetric and prolate. Thus, we combined the second and third eigenvalues into a single measure of the fiber tract radial diffusivity that represents the apparent diffusion coefficient perpendicular to the longitudinal axis of the fiber tract. This radial diffusivity is much lower than the diffusivity along the axis of the tract (λ_1) because the axon cell membranes and myelin sheaths add impediments to the diffusion perpendicular to the tract, resulting in a lower apparent diffusion coefficient (25).

The eigenvalue analysis clarifies the observed FA and MD effects in the temporal segment of the corpus callosum. All readers have essentially the same diffusivity in the PDD (along the left–right axis of the brain). Children with low phonological awareness and reading scores have lower radial diffusivity than good readers; hence, they have higher FA and lower MD than the good readers. As phonological awareness scores increase, radial diffusivity increases, leading to a lower FA and higher MD.

We illustrate this relationship in Fig. 3. The data points are the phonological awareness scores plotted against the average of the second and third eigenvalues, the fiber tract radial diffusivity. The icons at the right show the changing diffusion pattern when the first eigenvalue is fixed and the other two eigenvalues vary together. The magnitude of this tensor shape difference corresponds to the magnitude of the radial diffusivity difference observed at high and low phonological awareness.

Discussion

In highly coherent tissue like the corpus callosum, diffusivity along the axonal direction (the first eigenvalue of the diffusion tensor) is mainly determined by the intracellular "gel" (25, 26). The radial diffusivity (the second and third eigenvalues) depends significantly on the cell membranes and myelin sheaths (27), which form effective barriers to water diffusion. The diffusion pattern shown in Fig. 2 suggests that the intracellular milieu of the axons (axoplasm) in the temporal-callosal segment does not differ with phonological awareness and reading. But the diameter, density, and/or membrane properties of these axons, which determine the radial diffusivity, do correlate with these behavioral measures.

The specificity of the phonological awareness effect to radial diffusivity of the temporal-callosal fiber tract may be explained in at least two ways. One possibility is that the membranes and myelin

sheaths are more permeable to diffusing water in individuals with high phonological awareness. A second possibility, which we favor, is that there is a higher proportion of large axons in the good readers and thus a lower density of cell membranes in the perpendicular direction. This second interpretation is consistent with research that suggests that poor readers have difficulty processing visual and auditory stimuli that change quickly over time (28–30) because larger axons can conduct signals more quickly than smaller axons (31). Taken together with the lack of a correlation between reading and the overall size of the temporal-callosal segment ($r < 0.1$), this axon size and density interpretation also suggests that good readers have fewer total callosal connections passing through this part of the callosum. This reduced connectivity is consistent with data that suggest that poor readers have reduced hemispheric specialization in temporal lobe language regions (32, 33) because hemispheric specialization is related to reduced interhemispheric communication (20, 21). It is also consistent with the hypothesis that callosal differences are related to other gross morphological differences in good and poor readers (34).

We must note, however, that the specific cortical projection zones of our temporal-callosal segment are currently unknown. This particular callosal segment is especially difficult to track to cortex because of a consistent bias in the tensor data where these callosal pathways interdigitate with the inferior longitudinal fasciculus (see *Methods*).

Klingberg *et al.* (6) found a statistically reliable difference between groups of good and poor readers in a temporal-parietal region that they believed to be within the arcuate fasciculus, a component of the superior longitudinal fasciculus. This group difference was bilateral, but a portion of the voxels in only the left temporal-parietal volume of interest further correlated with individual word identification scores. The left arcuate fasciculus is long known for its role as the main pipeline between posterior and anterior language regions. The FA difference was thus interpreted by Klingberg *et al.* (6) as a "plausible structural basis for the functional disconnection of temporoparietal and frontal cortices that has been previously suggested to occur in developmental dyslexia."

All three replications of the result of Klingberg *et al.* placed the reading-related FA difference primarily within the corona radiata rather than the nearby arcuate fasciculus (7–9). The data in this study also confirm a reading-related FA difference in the left corona radiata when using a whole-brain correlation analysis as in Beaulieu *et al.* (8) (analysis not shown). Although adjacent to the arcuate, the corona radiata is thought to be different in terms of functionality. The posterior corona radiata is the continuation of the posterior limb of the internal capsule as it makes its way to sensorimotor cortex in and near the central sulcus. It contains axons primarily involved in low-level motor function. The integration of this finding with existing theories of reading development and dyslexia is therefore less straightforward. In an attempt to resolve this issue, Beaulieu *et al.* (8) suggest that, "although fibers from the [posterior limb of the internal capsule] pass right through the cluster, it is conceivable that other relevant white matter fibers crossing at this level, such as the adjacent superior longitudinal fasciculus, could be responsible for the correlation with reading ability." In other words, crossing fibers from adjacent structures may change the anisotropy in temporoparietal white matter voxels and underlie the correlation between FA and reading.

All but one of these studies used voxel-based analyses to potentially analyze the entire brain, yet none of them reported an FA difference in the corpus callosum. This null result is likely because of the extremely poor statistical power in the many white matter regions, including the corpus callosum, when using these methods (22). The one study that used an ROI-based analysis did not analyze the callosum (9).

A difference in the PDD between good and poor readers also has been reported (24). The PDD difference lies at the junction between anterior corona radiata and frontal-callosal pathways, several centimeters anterior to the posterior corona radiata.

Table 3. Descriptive statistics for the group of 49 children

	Mean	SD	Range
Age (years)	9.8	1.5	7.0–11.9
SES (Hollingshead)	45	14	17–66
Conners' ADHD T score (CPRS-Rs)	50.3	4.7	42–63
Letter-word ID (WJ-III)	106	14.5	70–136
Word attack (WJ-III)	106	11.5	78–128
Passage comprehension (WJ-III)	102	11.2	81–133
Phonological awareness (CTOPP)	100	13.2	73–133
Rapid naming (CTOPP)	99	12.6	79–130
Phonological memory (CTOPP)	99	10.5	79–130
GORT-4 Reading Quotient	105	20.3	64–148
WISC–IV Full-Scale IQ	111	13.5	85–145

All measures except the first three are age-normed standard scores (population mean, 100; SD, 15). SES, Hollingshead index of socioeconomic status (51).

Conclusions

There is a white matter region in the splenium of the corpus callosum where radial diffusivity is correlated with phonological awareness and reading. Radial diffusivity in the posterior callosal fibers of poor readers is lower, and FA is correspondingly higher compared with that of good readers. Several physiological mechanisms could cause this difference; a possibility we favor is that good readers have a higher proportion of large-diameter axons and fewer total axons passing through this part of the callosum. On this hypothesis, poor readers have denser interhemispheric coupling so that this interpretation is consistent with the increased functional symmetry observed in poor readers (32, 33). This interpretation of our results may also help to explain the decreased FA in posterior corona radiata reported for poor readers. A greater number of callosal axons in poor readers would be expected to reduce the FA (because of increased fiber crossings) in this part of the brain. Finally, the increased number of fibers may elongate the corona radiata, producing the anterior corona radiata effect reported in Schwartzman *et al.* (24).

Methods

Fifty-five children aged 7–12 participated in this study. The data described here represent the first measurement in a longitudinal study of reading development. All subjects were physically healthy and had no history of neurological disease, head injury, attention deficit/hyperactivity disorder (ADHD), language disability, or psychiatric disorder. In addition to screening for a history of ADHD, we also collected a quantitative measure of ADHD symptoms (Conners' Parent Rating Scale, Revised, short-form) and confirmed that all subjects scored in the normal range (<65). All subjects were native English speakers and had normal or corrected to normal vision and normal hearing. The Stanford Panel on Human Subjects in Medical and Non-Medical Research approved all procedures. Written informed consent/assent was obtained from all parents and children.

Data from five children were excluded because of imaging artifacts, including image distortion from dental work and excessive head motion. Data from one additional subject were excluded because the segmentation results from the two hemispheres (described below in *Callosal Segmentation*) were disparate. Thus, the results presented below are based on 49 of the 55 subjects. Of these 49 subjects, 21 were male.

Behavioral Testing. All subjects completed a 4-h battery of cognitive tests to characterize reading, phonological awareness, rapid naming,

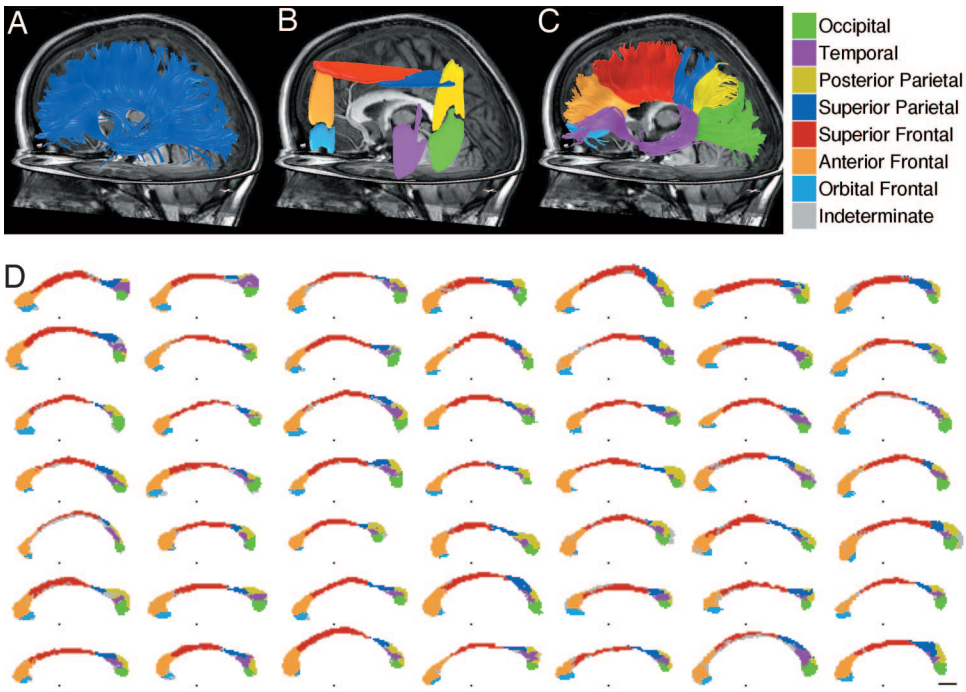

Fig. 4. Pathway selection. (*A*) All pathways in the right and left hemisphere are estimated; only those pathways that pass through the corpus callosum are analyzed. (*B*) The callosal pathways are segmented based on their intersection with one of seven possible planar regions, shown as the colored planes. (*C*) The segmentation of all the callosal pathways is shown by using the same color scheme as the planar segmentation regions. These are occipital (green), posterior parietal (yellow), superior parietal (blue), temporal (purple), superior frontal (red), anterior frontal (orange), orbitofrontal (cyan). (*D*) The outline of the callosum is color coded by the projection zone of the fibers within each segment. The black point below each corpus callosum indicates the location of the AC. The mean (SD) cross-sectional segment areas are as follows (in mm^2): occipital, 39.9 (10.8); temporal, 29.2 (14.4); posterior parietal, 30.7 (14.7); superior parietal, 33.5 (15); superior frontal, 103.8 (23.4); anterior frontal, 96.4 (20.8); orbital, 20.6 (8.5). All brains are AC–PC aligned, but otherwise left in native space. (Scale bar: 1 cm.)

and general intelligence. Table 3 summarizes the scores on these tests. As expected, phonological awareness (measured by the elision and blending subtests of the CTOPP) and word reading (measured by the WJ-III Basic Reading Composite score) were significantly correlated ($r = 0.72$; $P < 10^{-8}$).

DTI. DTI data were acquired on 1.5T Signa LX (Signa CVi; GE Medical Systems, Milwaukee, WI) by using a self-shielded, high-performance gradient system capable of providing a maximum gradient strength of 50 mT/m at a gradient rise time of 268 μs for each of the gradient axes. A standard quadrature head coil, provided by the vendor, was used for excitation and signal reception. Head motion was minimized by placing cushions around the head and securing a Velcro strap across the forehead.

The DTI protocol used eight 90-sec whole-brain scans; these were averaged to improve signal quality. The pulse sequence was a diffusion-weighted, single-shot, spin-echo, echo-planar imaging sequence (echo time, 63 msec; repetition time, 6 sec; field of view, 260 mm; matrix size, 128 × 128; bandwidth, ±110 kHz; partial k-space acquisition). We acquired 48–54 axial, 2-mm-thick slices (no skip) for two *b*-values, $b = 0$ and $b \approx 800$ sec/mm^2. The high *b*-value was obtained by applying gradients along 12 different diffusion directions (six noncollinear directions). Two gradient axes were energized simultaneously to minimize echo time. The polarity of the effective diffusion-weighting gradients was reversed for odd repetitions to reduce cross-terms between diffusion gradients and imaging and background gradients.

DTI data were preprocessed by using a custom program based on normalized mutual information that removed eddy current distortion effects and determined a constrained nonrigid image registration (35). The six elements of the diffusion tensor were determined by multivariate regression (36, 37). The eigenvalue decomposition of the diffusion tensor was computed, and the FA was calculated by using the resulting eigenvalues (36, 37). The FA is the normalized standard deviation of the three eigenvalues and indicates the degree to which the isodiffusion ellipsoid is anisotropic (i.e., one or two eigenvalues is larger than the mean of all three eigenvalues). The MD is the mean of the three eigenvalues, which is equivalent to one-third of the trace of the diffusion tensor.

For each subject, the T2-weighted ($b = 0$) images were coregistered to the T1-weighted 3D spoiled gradient-recalled acquisition in steady-state (SPGR) anatomical images. The coregistration was initiated by using the scanner coordinates stored in the image headers to achieve an approximate alignment. This alignment was refined by using a mutual-information 3D rigid-body coregistration algorithm from SPM2 (38). Several anatomical landmarks, including the anterior commissure (AC), the posterior commissure (PC), and the midsagittal plane, were identified by hand in the T1 images. With these landmarks, we computed a rigid-body transform from the native image space to the conventional AC–PC aligned space. The DTI data were then resampled to this AC–PC aligned space with 2-mm isotropic voxels by using a spline-based tensor interpolation algorithm (39), taking care to rotate the tensors to preserve their orientation with respect to the anatomy (40). The T1 images were resampled to the AC–PC aligned space with 1-mm isotropic voxels. We confirmed by visual inspection of each data set that this coregistration technique aligns the DTI and T1 images to within 1–2 mm in the brain regions of interest. However, the well known geometric distortions inherent in echo-planar imaging acquisition limit the accuracy in regions prone to susceptibility artifacts, such as orbitofrontal and anterior temporal regions.

Callosal Segmentation. We segmented the corpus callosum in each individual's brain based on the cortical projection zone of the fibers by using a modification of the procedure described by Huang *et al.* (41). The procedure is initiated by whole-brain fiber tracking that

produces multiple fiber paths. Fiber tracts were estimated by using a deterministic streamlines tracking algorithm (42–44) with a fourth-order Runge–Kutta path integration method (45) and 1-mm fixed-step size. A continuous tensor field was estimated by using trilinear interpolation of the tensor elements. Path tracing proceeded until the FA fell <0.15 or until the minimum angle between the current and previous path segments was $>30°$. Starting from the initial seed point, fibers were traced in both directions along the principal diffusion axis.

Fibers were estimated separately for each hemisphere. For example, the process for an individual's left hemisphere would consist of the following: (*i*) seeding the white matter of the left hemisphere, (*ii*) tracking fibers from these seeds, and (*iii*) selecting only those fibers that cross the corpus callosum. By tracking fibers from seeds in each hemisphere separately, we obtain two independent estimates of the callosal fascicles. We used these independent estimates to confirm the integrity of the data and the validity of the methods (22, 46). The results from the two hemispheres were very similar for all 49 subjects, and fiber estimates were merged for all subsequent analyses. An example of the callosal estimates in one brain is shown in Fig. 4*A*.

The callosal segmentation procedure relies on a set of manually defined ROIs within the white matter. We draw these ROIs in each brain and identify those callosal fibers that intersect them (Fig. 4*B*). The ROIs are chosen so that the fiber bundles fall into compact regions that partition and cover the corpus callosum. The ROIs used by Huang *et al.* (41) produce a segmentation that is too coarse for our purposes; for example, their method does not distinguish anterior parietal fibers that are destined for postcentral gyrus (presumably carrying somatosensory information) from the more posterior parietal fibers (presumably carrying visual information). Therefore, we subdivided their ROIs to distinguish between superior-parietal and posterior-parietal regions. The ROIs that we used produce seven distinct callosal segments: occipital, temporal, superior parietal, posterior parietal, superior frontal, anterior frontal, and orbital frontal. The corresponding fiber groups are shown in Fig. 4*C*. Note that many of the "temporal" pathways actually terminate in the lateral frontal lobe. This error is due to a consistent bias in DTI data acquired at this resolution in the region where the temporal fibers interdigitate with the occipitofrontal fasciculus (46, 47). Such a bias is the primary motivation for following the parcellation method of Huang *et al.* (41) rather than methods based on cortical surface ROIs. By placing the ROIs in the white matter close to the callosum, we catch pathways before they wander astray.

The custom software used for all of the analysis and visualization can be obtained from the authors on request.

The resulting callosal parcellations for all 49 subjects are shown in Fig. 4*D*. This midsagittal classification was computed for each voxel by (*i*) counting how many fibers of each of the seven fiber groups passed through that voxel, and (*ii*) assigning the voxel to the category with the most fibers. Voxels with no fibers passing through them were assigned to an eighth group ("indeterminate"). Had there been voxels with equal numbers from more than one group, they would have been randomly assigned to one of the groups.

Although the callosal parcellation methods used here are relatively new, the results that they produce are in close agreement with the extensive monkey literature (48) and the limited human data (49).

This work was supported by National Institutes of Health Grant EY015000 and the Dana Foundation.

1. Shaywitz BA, Shaywitz SE, Pugh KR, Mencl WE, Fulbright RK, Skudlarski P, Constable RT, Marchione KE, Fletcher JM, Lyon GR, *et al.* (2002) *Biol Psychiatry* 52:101–110.
2. Shaywitz SE, Shaywitz BA, Pugh KR, Fulbright RK, Constable RT, Mencl WE, Shankweiler DP, Liberman AM, Skudlarski P, Fletcher JM, *et al.* (1998) *Proc Natl Acad Sci USA* 95:2636–2641.
3. Temple E (2002) *Curr Opin Neurobiol* 12:178–183.
4. Eden GF, VanMeter JW, Rumsey JM, Maisog JM, Woods RP, Zeffiro TA (1996) *Nature* 382:66–69.
5. Demb JB, Boynton GM, Heeger DH (1997) *Proc Natl Acad Sci USA* 94:13363–13366.
6. Klingberg T, Hedehus M, Temple E, Salz T, Gabrieli JD, Moseley ME, Poldrack RA (2000) *Neuron* 25:493–500.
7. Deutsch GK, Dougherty RF, Bammer R, Siok WT, Gabrieli JD, Wandell B (2005) *Cortex* 41:354–363.
8. Beaulieu C, Plewes C, Paulson LA, Roy D, Snook L, Concha L, Phillips L (2005) *NeuroImage* 25:1266–1271.
9. Niogi SN, McCandliss BD (2006) *Neuropsychologia* 44:2178–2188.
10. Orton S (1939) *Education Record* 12:58–68.
11. Geschwind N, Galaburda AM (1985) *Arch Neurol* 42:428–459.
12. Galaburda AM (1992) *Curr Opin Neurol Neurosurg* 5:71–76.
13. Rumsey JM (1992) *J Am Med Assoc* 268:912–915.
14. Rumsey JM, Andreason P, Zametkin AJ, Aquino T, King AC, Hamburger SD, Pikus A, Rapoport JL, Cohen RM (1992) *Arch Neurol* 49:527–534.
15. Habib M (2000) *Brain* 123:2373–2399.
16. Geschwind N, Behan P (1982) *Proc Natl Acad Sci USA* 79:5097–5100.
17. Rumsey JM, Casanova M, Mannheim GB, Patronas N, De Vaughn N, Hamburger SD, Aquino T (1996) *Biol Psychiatry* 39:769–775.
18. Robichon F, Habib M (1998) *Brain Lang* 62:127–146.
19. von Plessen K, Lundervold A, Duta N, Heiervang E, Klauschen F, Smievoll AI, Ersland L, Hugdahl K (2002) *Neuropsychologia* 40:1035–1044.
20. Witelson SF (1985) *Science* 229:665–668.
21. Rosen GD, Sherman GF, Galaburda AM (1989) *Neuroscience* 33:525–533.
22. Dougherty RF, Ben-Shachar M, Deutsch G, Potanina P, Bammer R, Wandell BA (2005) *Ann NY Acad Sci* 1064:98–112.
23. Witelson SF (1989) *Brain* 112:799–835.
24. Schwartzman A, Dougherty RF, Taylor JE (2005) *Magn Reson Med* 53:1423–1431.
25. Beaulieu C (2002) *NMR Biomed* 15:435–455.
26. Sehy JV, Ackerman JJ, Neil JJ (2002) *Magn Reson Med* 48:765–770.
27. Sen PN, Basser PJ (2005) *Biophys J* 89:2927–2938.
28. Tallal P, Merzenich MM, Miller S, Jenkins W (1998) *Exp Brain Res* 123:210–219.
29. Stein J (2001) *Dyslexia* 7:12–36.
30. Livingstone MS, Rosen GD, Drislane FW, Galaburda AM (1991) *Proc Natl Acad Sci USA* 88:7943–7947.
31. Rushton WA (1951) *J Physiol* 115:101–122.
32. Simos PG, Fletcher JM, Bergman E, Breier JI, Foorman BR, Castillo EM, Davis RN, Fitzgerald M, Papanicolaou AC (2002) *Neurology* 58:1203–1213.
33. Shaywitz BA, Shaywitz SE, Blachman BA, Pugh KR, Fulbright RK, Skudlarski P, Mencl WE, Constable RT, Holahan JM, Marchione KE, *et al.* (2004) *Biol Psychiatry* 55:926–933.
34. Eckert M (2004) *Neuroscientist* 10:362–371.
35. Bammer R, Auer M (2001) in *Proceedings of the Ninth Annual Meeting of ISMRM* (International Society for Magnetic Resonance in Medicine, Glasgow, UK), Vol 9, p 508.
36. Basser PJ (1995) *NMR Biomed* 8:333–344.
37. Basser PJ, Pierpaoli C (1996) *J Magn Reson B* 111:209–219.
38. Friston K, Ashburner J (2004) *NeuroImage* 23:21–24.
39. Pajevic S, Aldroubi A, Basser PJ (2002) *J Magn Reson* 154:85–100.
40. Alexander DC, Pierpaoli C, Basser PJ, Gee JC (2001) *IEEE Trans Med Imaging* 20:1131–1139.
41. Huang H, Zhang J, Jiang H, Wakana S, Poetscher L, Miller MI, van Zijl PC, Hillis AE, Wytik R, Mori S (2005) *NeuroImage* 26:195–205.
42. Basser PJ, Pajevic S, Pierpaoli C, Duda J, Aldroubi A (2000) *Magn Reson Med* 44:625–632.
43. Conturo TE, Lori NF, Cull TS, Akbudak E, Snyder AZ, Shimony JS, McKinstry RC, Burton H, Raichle ME (1999) *Proc Natl Acad Sci USA* 96:10422–10427.
44. Mori S, Crain BJ, Chacko VP, van Zijl PC (1999) *Ann Neurol* 45:265–269.
45. Press WH, Teukolsky SA, Vetterling WT, Flannery BP (2002) *Numerical Recipes in C++: The Art of Scientific Computing* (Cambridge Univ Press, Cambridge, UK).
46. Dougherty RF, Ben-Shachar M, Bammer R, Brewer AA, Wandell BA (2005) *Proc Natl Acad Sci USA* 102:7350–7355.
47. Dougherty RF, Deutsch GK, Ben-Shachar M, Potanina P, Bammer R, Wandell BA (2005) *Soc Neurosci Abstr* 31:354.4.
48. Schmahmann JD, Pandy DN (2006) *Fiber Pathways of the Brain* (Oxford Univ Press, New York).
49. de Lacoste MC, Kirkpatrick JB, Ross ED (1985) *J Neuropathol Exp Neurol* 44:578–591.
50. Krynicki K, Green CD, Sawyer DW (1978) *Faraday Discuss Chem Soc* 66:199–208.
51. Hollingshead AB (1975) *Four Factor Index of Social Skills* (Yale Univ Press, New Haven, CT).